ability to associate with several integral membrane proteins, such as CD43, CD44, intercellular adhesion molecule (ICAM)-1, ICAM-2, ICAM-3, and the H^+/K^+ ATPase pump (Bretscher et al., 1997; Heiska et al., 1998; Hirao et al., 1996; Serrador et al., 1997; Tsukita et al., 1994; Tsukita and Yonemura, 1999; Yonemura et al., 1993). Conversely, the COOH-terminal halves of ERM proteins can interact with actin filaments (Bretscher et al., 1997; Tsukita and Yonemura, 1999; Turunen et al., 1994). As the NH2-terminal halves of ERM proteins can also bind to their COOH-terminal halves (Andreoli et al., 1994; Bretscher et al., 1997; Tsukita and Yonemura, 1999), both the actin- and membrane-binding domains of ERM proteins are thought to be masked in the resting state by an intramolecular and/or intermolecular head-to-tail association (Berryman et al., 1995; Bretscher et al., 1995; Bretscher et al., 1997; Tsukita and Yonemura, 1999). These dormant ERM proteins are thought to be activated by cellular signals, such as the one mediated by epidermal growth factor receptor, by exposing their halves and allowing them to interact with integral membrane proteins and actin filaments, respectively (Berryman et al., 1995; Bretscher et al., 1995; Bretscher et al., 1997; Hirao et al., 1996; Matsui et al., 1998; Tsukita and Yonemura, 1999). These activated ERM proteins have been shown to be directly involved in the morphogenesis of the free surface domain of plasma membranes, especially in the organization of microvilli (Berryman et al., 1995; Bretscher et al., 1997; Chen et al., 1995; Crepadi et al., 1997; Kondo et al., 1997; Takeuchi et al., 1994; Tsukita and Yonemura, 1999).

In this study, we investigated the effect of Stx1-B binding to Gb3 on ACHN cells and found that an intracellular signal mediated by Gb3 induces the phosphorylation of ezrin proteins, leading to a reorganization of the cytoskeleton and morphological changes. Our findings should improve our understanding of the molecular mechanism of Stx-mediated cell damage and the functional roles of Gb3-mediated intracellular signals in a physiological context.

Materials and Methods

Materials

The Stx1-B pentamer was prepared as described previously (Nakajima et al., 2001). The mouse monoclonal antibodies (mAbs) used in this study were obtained from BD Biosciences (Lexington, KY) (anti-ezrin, anti-paxillin and anti-Yes), Immunotech (Fullerton, CA) (anti-CD44 and anti-cytokeratin), Affinity BioReagents, Inc. (ABR, Golden, CO) (anti-vimentin), Santa Cruz Biotechnology (Santa Cruz, CA) (anti-actin), and Sigma-Aldrich Fine Chemicals (St Louis, MO) (anti-α Tubulin). The mouse anti-Gb3 mAb 1A4 was a generous gift of S. Hakomori of the University of Washington (Seattle, WA) and Otsuka Assay Laboratories (Kawauchi-cho, Tokushima, Japan). The rat anti-Gb3 mAb 38.13 were obtained from Immunotech. The polyclonal Abs were obtained from Upstate biotechnology (Lake Placid, NY) (anti-FAK), New England Biolabs, (Bevely, MA) (anti-phospho-specific ezrin and anti-phospho-specific paxillin), ABR (anti-phospho-specific Src) and Sigma (anti-γ Tubulin). Peroxidase-conjugated secondary Abs were purchased from DAKO (Glostrup, Denmark). Fluorescence-conjugated secondary Abs and fluorescence labeling reagents for the primary Abs were purchased from Molecular Probes, Inc. (Eugene, OR). The Rho-dependent serine/threonine kinase (ROCK) inhibitor Y-27632, PI 3 kinase (PI3K) inhibitor LY-294002, protein kinase C (PKC) inhibitor 20-28, PKC inhibitor EGF-R fragment 651-658, and Src family protein tyrosine kinase (PTK) inhibitor PP2 were purchased from Calbiochem-Novabiochem (San Diego, CA). Methyl-β-cyclodextrin (MBD) and DAPI were obtained from Sigma. TRITC-conjugated phalloidin was purchased from Molecular Probes. Cell-tracker Green was also purchased from Molecular Probes. Other chemical reagents were obtained from Wako Pure Chemical Industries (Osaka, Japan), unless otherwise indicated.

Cell culture

Renal tubular epithelial carcinoma-derived ACHN cells that were sensitive to Stx1 cytotoxicity (Katagiri et al., 1999; Taguchi et al., 1998) were used in this study. The cells were maintained in DMEM supplemented with 10% FCS at 37°C in a humidified 5% CO_2 atmosphere. Cells were grown to approximately 75% confluence and stimulated. In most of the experiments, Stx1-B pentamer was directly added to the culture medium at a concentration of 5.0 μg/ml and cells were incubated for the time periods indicated in the figures, unless otherwise indicated.

Immunohistochemistry and confocal microscopic analysis

To observe cell morphology, ACHN cells were plated on a polylysine-coated glass bottom dish (Matsunami Glass, Tokyo, Japan) and labeled with Cell-tracker Green, according to the manufacturer's protocol. For the immunohistochemical staining, the cells were plated on a collagen-coated cover slip (Iwaki Glass, Tokyo, Japan). After each treatment, cells on cover slips were washed with ice-cold PBS and fixed with ice-cold acetone for 20 minutes at 4°C, then stained with each combination of Abs and/or reagents described below.

For the simultaneous detection of ezrin and filamentous actin (F-actin), the cover slips were incubated with primary Abs against ezrin (5 μg/ml) at room temperature for 30 minutes followed by PBS washing. The cells were further incubated with secondary goat anti-mouse Ab labeled with Alexa Fluor® 488 (1:300 dilution) for 30 minutes, followed by PBS washing and then stained with DAPI (200 ng/ml) and TRITC-conjugated phalloidin (5 units/ml) (Knowles and McCulloch, 1992). The detection of CD44 and F-actin was performed similarly.

For the detection of paxillin and FAK, a combination of mouse anti-paxillin mAb and rabbit anti-FAK polyclonal Ab was used. Both primary Abs (5 μg/ml each) were detected by Alexa Fluor® 488-conjugated goat anti-mouse Ab and Alexa Fluor® 546-conjugated goat anti-rabbit Ab (1:300 each), respectively. Each secondary Ab was highly cross-absorbed, thus the cross reactions were not detected in preliminary experiments (data not shown). The detection of α- and γ-tubulin was performed similarly. For the simultaneous detection of vimentin and cytokeratin, each primary Ab was labeled using either the Alexa Fluor® 488 Protein Labeling Kit or the Zenon™ Alexa Fluor® 546 Mouse IgG1 Labeling Kit.

Confocal laser scanning was performed using a FV500 confocal laser scanning microscope (Olympus, Tokyo, Japan). Simultaneous multi-fluorescence acquisitions were performed using the 351 nm, 488 nm, and 543 nm laser lines to excite DAPI, Alexa Fluor™488, and Alexa Fluor™546 (TRITC), respectively, using a water-immersion objective (×40, NA1.7). Fluorescent images were selected using appropriate multi-fluorescence dichroic mirrors and band pass filters using the sequential acquisition mode.

Immunoblot analysis

For the immunoblot analysis, ACHN cells were plated on a 100 mm culture dish (Corning, Corning, NY). Cell lysates were prepared by solubilizing cells in 400 μl of lysis buffer, and the protein concentration of each cell lysate was determined as described previously (Kiyokawa et al., 2001). 50 μg of each whole cell lysate was electrophoretically separated on an SDS-polyacrylamide gel and transferred to a nitrocellulose membrane using a semi-dry transblot system (Bio-Rad Laboratories, Hercules, CA). Immunoblotting was performed as described previously (Kiyokawa et al., 2001).

Actin and tubulin polymerization assay

Quantification of actin polymerization was carried out essentially as described previously with minor modifications (Heacock and Bamburg, 1983; Glogauer et al., 1997; McCormack et al., 1999). Briefly, ACHN cells were plated in quintuple wells of a 6-well culture dish (Corning) at 1.5×10^5 cells in 5 ml of medium, and grown for 40 hours to achieve approximately 75% confluence, and treated with 5.0 µg/ml of Stx1-B pentamer for the time periods indicated in the figures. At the end of the incubation period, cells were washed in ice-cold PBS and quickly lysed in 500 µl of actin stabilization buffer (Heacock and Bamburg, 1983; McCormack et al., 1999), a buffer that stabilizes both monomer actin (G-actin, soluble) and F-actin (polymerized) pools. Aliquots of 50 µl from each original (whole) lysate were removed and stored for the determination of total actin. The cell lysates were immediately centrifuged at room temperature for 1 minute in a microcentrifuge at 10,000 *g*, after which the supernatants (G-actin) were removed from the pellets (F-actin). Then 450 µl of actomyosin extraction buffer (Heacock and Bamburg, 1983) was added to the solid pellets. Aliquots of 5 µl from both original lysates (total actin) and resuspended pellets (F-actin) were examined by immunoblot analysis using anti-actin mAb and quantified by densitometry (Glogauer et al., 1997). The proportion of F-actin to total actin was calculated and shown as a percentage.

Quantification of tubulin polymerization was examined essentially the same as actin polymerization with some exceptions. First, the original lysates were prepared by using specific lysis buffer for tubulin and centrifuged at 10,000 *g* for 10 minutes as described elsewhere (Minotti et al., 1991; Montgomery et al., 2000). Second, after removal of the supernatants containing soluble tubulin, solid pellets containing polymerized tubulin were resuspended in water (Minotti et al., 1991; Montgomery et al., 2000). Third, immunoblot analysis was performed with anti-α tubulin mAb.

Results

Morphological changes in ACHN cells induced by Stx1-B treatment

We previously observed, during a study on the biological function of the Stx1-B subunit, that Stx1-B treatment induces a weakening in the adhesion of ACHN cells to the culture dish (Katagiri et al., 2001). As the same phenomenon is also observed in primary cultures of normal human renal cortical epithelial cells (data not shown), it is likely that this is a common feature observed in renal epithelial-derived cells mediated by Stx1-B-induced intracellular signals.

To examine the effect of Stx1-B on the adhesiveness of ACHN cells in greater detail, we stained the cells with Cell-tracker Green and observed the morphological changes using confocal laser scanning microscopy. As shown in Fig. 1, the addition of Stx1-B to the culture weakened the adhesiveness of the cells, as recognized by the increase in intracellular spaces in a time-dependent manner and by the morphological changes, in which the cells became smaller and rounder. In addition, filopodia- and lamellipodia-like structures were temporarily observed after Stx1-B treatment (Fig. 1, arrowhead).

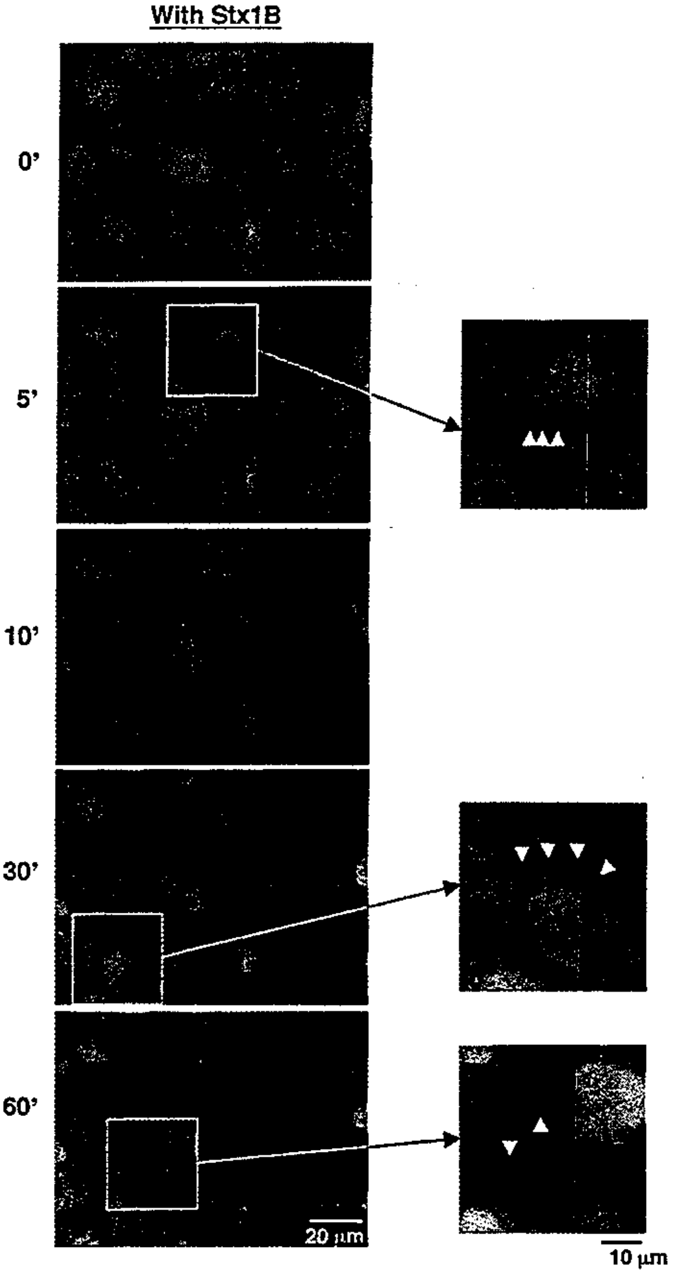

Fig. 1. Morphological changes in ACHN cells after treatment with the Stx1-B subunit. ACHN cells stained with Cell-tracker Green were treated with and without 5 µg/ml of the Stx1-B subunit for the indicated periods and visualized using confocal microscopy. Filopodia- and lamellipodia-like structures are visible at higher magnifications and are indicated by the arrowheads. Results are representative of three independent experiments.

Stx1-B induces the redistribution of cytoskeletal proteins in ACHN cells

The remodeling of cytoskeletal proteins, including the ERM family proteins and actin, is involved in the formation of filopodia or lamellipodia during morphological changes (Berryman et al., 1995; Bretscher et al., 1997; Chen et al., 1995; Crepadi et al., 1997; Kondo et al., 1997; Takeuchi et al., 1994; Tsukita and Yonemura, 1999). Therefore, we examined whether Stx1-B treatment affects the distribution of ezrin and actin. In the resting state, most of the ezrin protein was dispersed in the cytoplasm and only a portion of the protein

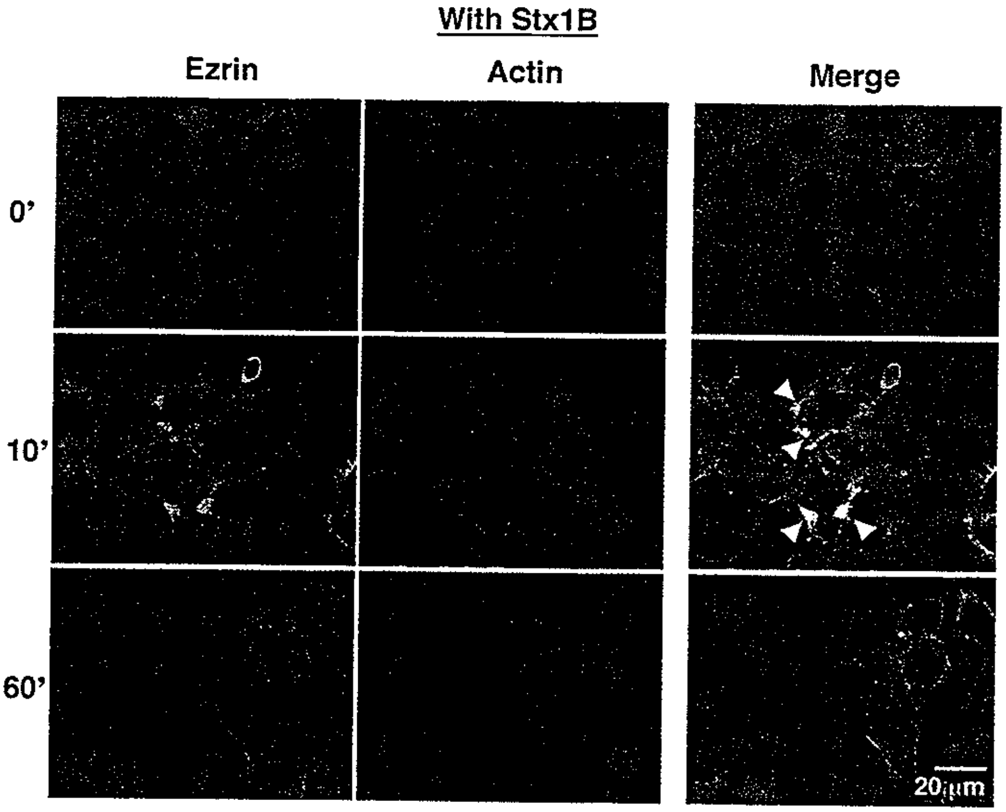

Fig. 2. Effect of Stx1-B subunit on the distribution of ezrin and actin in ACHN cells. ACHN cells treated with the Stx1-B subunit as described in Fig. 1 were double-stained with Alexa-488-labeled anti-ezrin mAb (left panels, green) and TRITC-phalloidin (center panels, red) and visualized using confocal microscopy. The right panels represent the superposition of the green and red images, with DAPI counter staining (blue). The arrowheads indicate the areas of ezrin and actin colocalization (yellow). Results are representative of five independent experiments.

was concentrated in the margin of the cells, as revealed by the brush-like meshwork (Fig. 2, top panels). However, Stx1-B treatment induced a transient enhancement in the concentration of ezrin just beneath the plasma membrane (Fig. 2). Occasionally, the protein clustering peaked at 10 minutes after Stx1-B stimulation (Fig. 2). In parallel, the cortical actin filaments were temporarily polymerized and appeared as thick bundles at the margin of the cells (Fig. 2). The colocalization of both proteins peaked at 10 minutes after Stx1-B stimulation (Fig. 2, yellow area, indicated by arrowhead).

As ERM proteins are thought to play a central role in the organization of cortical actin-based cytoskeletons through the cross-linking of actin filaments and integral membrane, such as CD44 (Tsukita et al., 1994; Tsukita and Yonemura, 1999), we next examined the changes in the distribution of CD44 induced by Stx1-B treatment. As with ezrin, Stx1-B treatment temporarily enhanced the concentration of CD44 in the cell membrane of ACHN cells (Fig. 3). Dual staining with CD44 and F-actin revealed a significant colocalization of both proteins that peaked at 10 minutes after Stx1-B stimulation (Fig. 3, yellow area, indicated by arrowhead).

Paxillin and FAK have been shown to be important for the focal adhesion of cells and growth factor-induced morphological changes (Burridge et al., 1992; Leventhal et al., 1997). Therefore, we examined the effect of Stx1-B stimulation on the distribution of FAK and paxilin. As shown in Fig. 4, most of the FAK and paxillin proteins were independently disseminated throughout the cytoplasm, while small portions of both proteins were colocalized and concentrated within a distinct radial streak at the edges of the cell lamella (yellow area). Upon the addition of Stx1-B, however, the colocalization of FAK and paxillin was temporally enhanced, peaking at 10 minutes after stimulation (Fig. 4, arrowhead).

We further examined the effect of Stx1-B stimulation on other cytoskeletal proteins. The distributions of vimentin and cytokeratin were similar, appearing as a diffuse localization with radial meshwork in the cytoplasm of resting ACHN cells (Fig. 5). Upon Stx1-B stimulation, however, both proteins were temporary concentrated within a paranuclear lesion, peaking at 30 minutes after stimulation in a synchronous manner (Fig. 5, arrowhead).

When the distribution of tubulins was examined using fluorescence immunohistochemistry, a fine mesh work of α-tubulin was seen within the cytoplasm of ACHN cells (Fig. 6). Upon Stx1-B stimulation, the α-tubulin filaments became significantly polymerized, appearing as a thickening of the bundles throughtout the entire cytoplasm and peaking at 10 minutes after stimulation (Fig. 6). Conversely, γ-tubulin was found in cytoplasmic complexes identified as fine spots and specifically concentrated at microtubule-organizing centers (Moritz and Agard, 2001) (Fig. 6). Although the distribution of γ-tubulin did not change significantly after Stx1-B stimulation, a slight enhancement at the microtubule-organizing centers was observed (Fig. 6, arrowhead).

All above observations on Stx1-B-induced cytoskeletal remodeling are entirely based on imaging studies. Therefore, we next examined F-actin formation after Stx1-B stimulation by biochemical means. For this purpose, cell lysate prepared by using actin stabilization buffer was centrifuged and F-actin fraction was separated from soluble G-actin fraction as the pellet. As shown in Fig. 7A, quantification by densitometry of

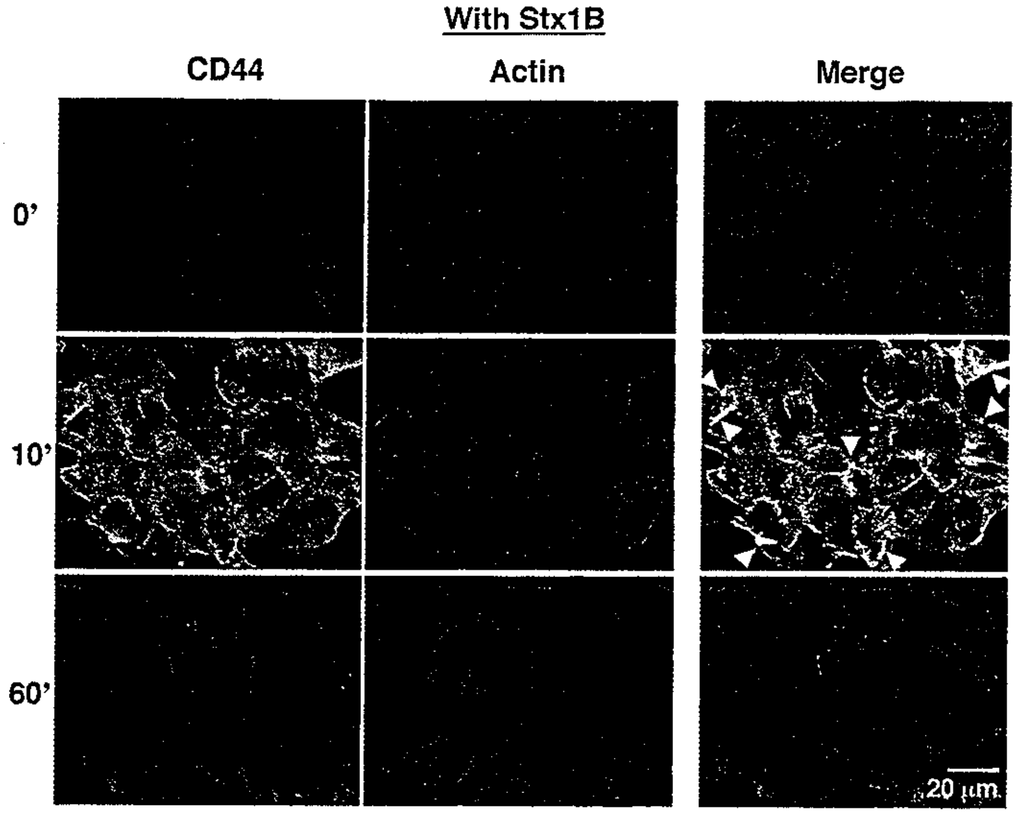

Fig. 3. Effect of Stx1-B subunit on the distribution of CD44 and actin in ACHN cells. ACHN cells were examined as described in Fig. 2 using Alexa-488-labeled anti-CD44 mAb (left panels, green) and TRITC-phalloidin (center panels, red). The arrowheads indicate the areas of CD44 and actin colocalization (yellow). Results are representative of three independent experiments.

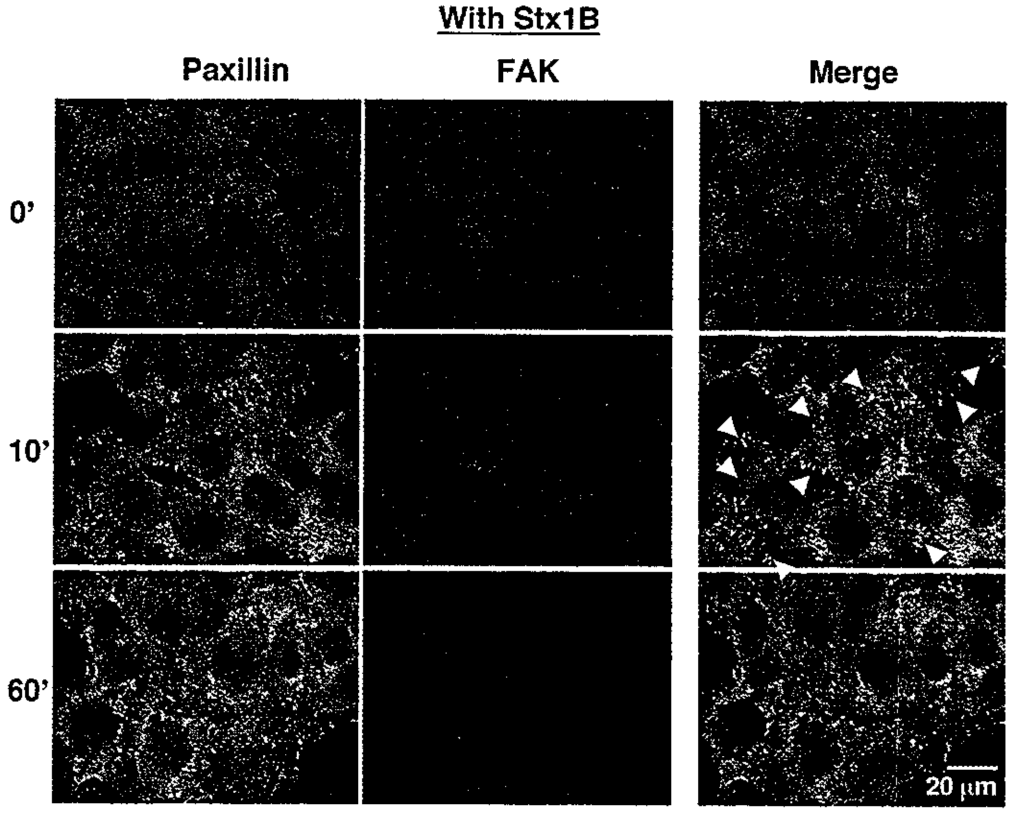

Fig. 4. Effect of Stx1-B subunit on the distribution of paxillin and FAK in ACHN cells. ACHN cells were examined as described in Fig. 2 using Alexa-488-labeled anti-paxillin mAb (left panels, green) and Alexa-546-labeled anti-FAK Ab (center panels, red). The arrowheads indicate the areas of paxillin and FAK colocalization (yellow). Results are representative of three independent experiments.

immunoblots revealed a transient increase in the amount of F-actin fraction, which peaked at 10 to 30 minutes after Stx1-B stimulation. These data coincide with those observed by confocal microscopy experiments using fluorescently labeled phalloidin as a probe for F-actin (Figs 2, 3). We also examined tubulin polymerization similarly. As shown in Fig. 7B, Stx1-

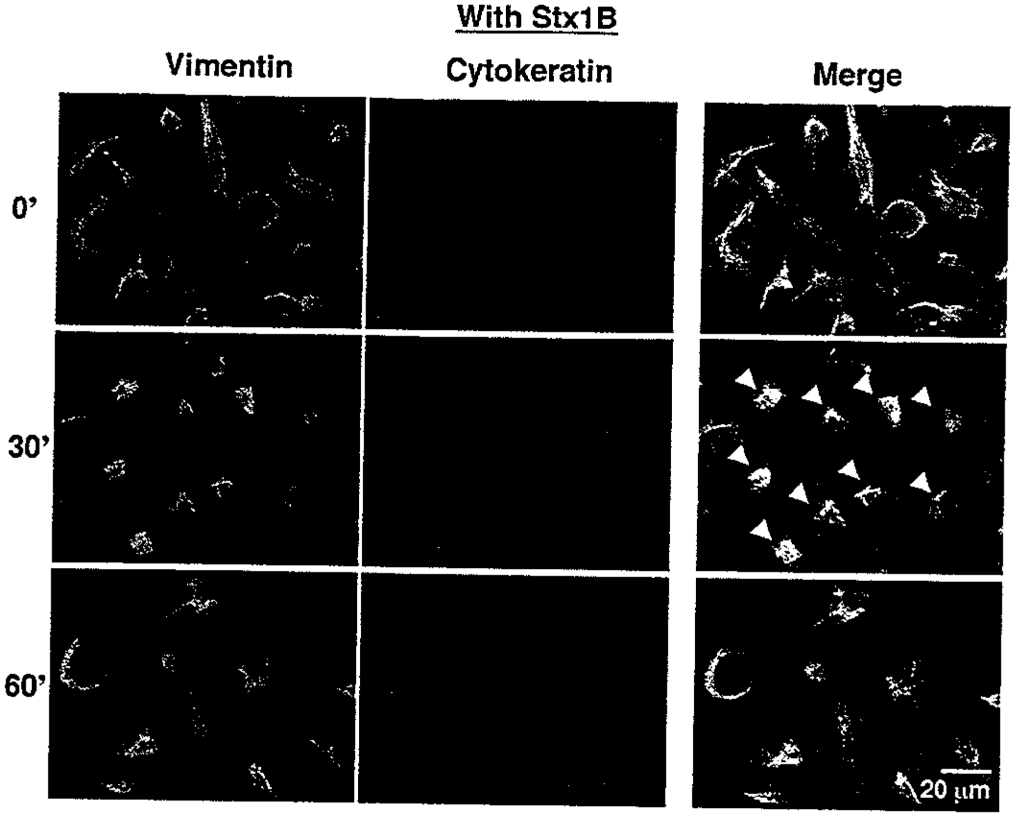

Fig. 5. Effect of Stx1-B subunit on the distribution of vimentin and cytokeratin in ACHN cells. ACHN cells were examined as described in Fig. 2 using Alexa-488-labeled anti-vimentin mAb (left panels, green) and Alexa-546-labeled anti-cytokeratin mAb (center panels, red). The arrowheads indicate the perinuclear clustering of vimentin. Results are representative of three independent experiments.

B-induced transient tubulin polymerization was also confirmed by quantitative analysis.

Stx1-B induces transient phosphorylation of ezrin

The phosphorylation of cytoskeletal proteins plays a key role in cytoskeletal remodeling (Tsukita and Yonemura, 1999). Thus, we attempted to examine whether the phosphorylation state of the cytoskeletal proteins changes. When the total cell lysates prepared from Stx1-B-treated ACHN cells were examined using immunoblotting with Abs that specifically recognize Src family PTKs only when activated by phosphorylation at the C-terminal tyrosine residue, the intensification of three major bands was seen after Stx1-B treatment (Fig. 8A). Based on the molecular weights, the largest band was thought to represent the activated form of Yes, which was previously reported to appear during the course of Stx1-B-mediated activation in ACHN cells (Katagiri et al., 1999; Katagiri et al., 2001). The other smaller bands were thought to represent the activation of other Src family PTK(s) by Stx1-B stimulation. In parallel with the activation of Src family PTKs, the Stx1-B-mediated phosphorylation of both ezrin and paxillin was detected by immunoblotting with Abs that specifically recognize the phosphorylated active forms of ezrin and paxillin (Fig. 8A). The above data indicate that the Stx1-B-mediated intracellular signal induces the phosphorylation of ezrin and paxillin during the course of cytoskeletal remodeling.

As shown in Fig. 8B, the effect of Stx1-B on the induction of ezrin phosphorylation is dose-dependent and the concentration of 1 μg/ml was found to be sufficient to yield maximum effect. As shown in Fig. 8C, we also found that the treatment with anti-Gb3 Abs similarly induces the phosphorylation of ezrin in ACHN cells. Therefore, the ligation of Gb3 by pentameric Stx1-B is not always required to induce cytoskeletal signaling and the binding of monomeric forms of the ligand to Gb3 might be able to induce ezrin phosphorylation.

We also examined whether constitutive Stx1-B treatment is required to induce ezrin phosphorylation. For this purpose, we bound Stx1-B to ACHN cells on ice and then removed excess toxin by washing, before shifting the temperature to 37°C. As shown in Fig. 8D, after the temperature was shifted to 37°C, transient increase in phosphorylation of ezrin was observed by immunoblotting. Although the elevation of ezrin phosphorylation observed in this experiment is slower than that presented in Fig. 8A, it is probably due to the time lag for warming up of the medium to 37°C after the temperature shift. These data indicate that the primary ligation of the plasma membrane Gb3 pool by Stx1-B is sufficient to induce intracellular signal for cytoskeletal rearrangements.

Effect of inhibitors on Stx1-B-induced cytoskeletal remodeling

To clarify the signaling cascade that induces the phosphorylation of ezrin, we examined the effect of a number of inhibitors on Stx1-B-induced ezrin phosphorylation. As shown in Fig. 9, when ACHN cells were pre-treated with PP2, a specific inhibitor for Src family PTK, the Stx1-B-mediated phosphorylation of ezrin was clearly inhibited. Similary, MBD, which is known to disturb the structure of the lipid rafts through the depletion of cholesterol from the cell membrane,

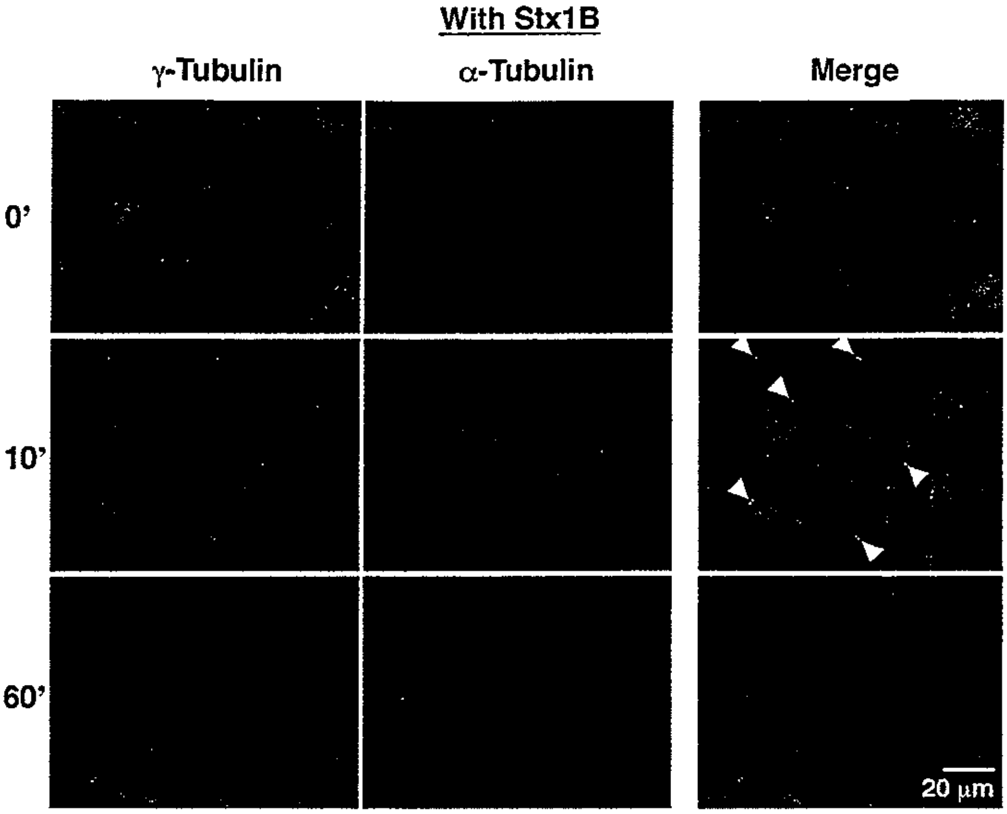

Fig. 6. Effect of Stx1-B subunit on the distribution of γ- and α-tubulins in ACHN cells. ACHN cells were examined as described in Fig. 2 using Alexa-488-labeled anti-γ-tubulin Ab (left panels, green) and Alexa-546-labeled anti-α-tubulin mAb (center panels, red). The arrowheads indicate the accumulation of γ-tubulin at the microtubule-organizing centers. Results are representative of three independent experiments.

inhibited the Stx1-B-mediated phosphorylation of ezrin (Fig. 9). In addition, LY294002, a specific inhibitor for PI3K, and Y27632, a specific inhibitor for ROCK, also inhibited the Stx1-B-mediated phosphorylation of ezrin (Fig. 9). In contrast, PKC inhibitor 20-28 (Fig. 9) and PKC inhibitor EGF-R fragment 651-658 (data not shown) did not affect the Stx1-B-mediated phosphorylation of ezrin in ACHN cells.

We next examined whether these inhibitors affect the Stx1-B-mediated cytoskeletal rearrangements. As shown in Fig. 2 and Fig. 10A, Stx1-B treatment induced the clustering of ezrin beneath the plasma membrane (indicated by arrowhead). When ACHN cells were pretreated with any of inhibitors, including PP2, MBD, LY294002 and Y27632, however, the Stx1-B-induced clustering of ezrin was not observed (Fig. 10A). Therefore, it is suggested that the inhibition of ezrin phosphorylation by these inhibitors suppresses Stx1-B-mediated redistribution of ezrin.

To clarify the molecule responsible for the redistribution of vimentin during the course of Stx1-B-induced cytoskeletal remodeling, we next examined the effect of inhibitors on the Stx1-B-induced redistribution of vimentin. As shown in Fig. 5 and Fig. 10B, Stx1-B treatment induced the accumulation of vimentin in the paranuclear area (indicated by arrowhead). When ACHN cells were pretreated with either PP2 or Y27632, however, the Stx1-B-induced clustering of vimentin in the paranuclear region was not observed (Fig. 10B), indicating the involvement of the Src family PTK and ROCK in the Stx1-B-mediated redistribution of vimentin.

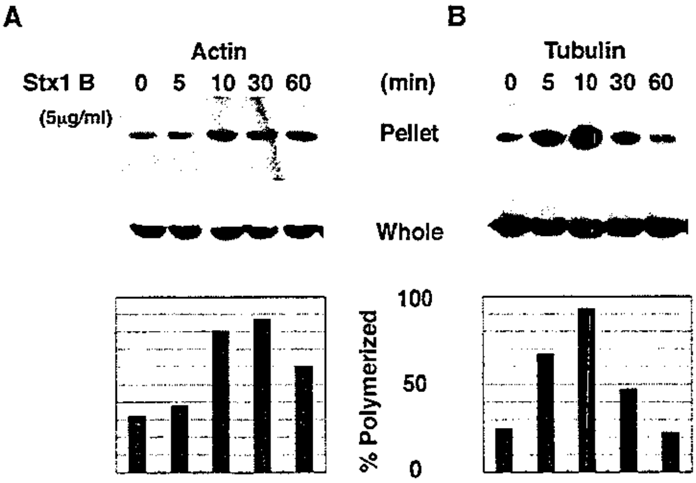

Fig. 7. Effect of Stx1-B subunit on the polymerization of actin and tubulin in ACHN cells. (A) ACHN cells were treated with and without 5 μg/ml of the Stx1-B subunit as described in Fig. 1 and lysed in the actin stabilization buffer. After removing aliquots from each whole lysate for the determination of total actin, polymerized actin (filamentous actin) was separated from soluble actin (monomer actin) by centrifugation. Both fractions of polymerized actin (pellet, upper panel) and total actin (whole, mid panel) were detected by immunoblot analysis and quantitated by densitometry. The proportion (%) polymerized was calculated by dividing the actin in the pellet fraction by the actin in the whole lysate and indicated (lower panel). (B) Tubulin polymerization was examined as in A.

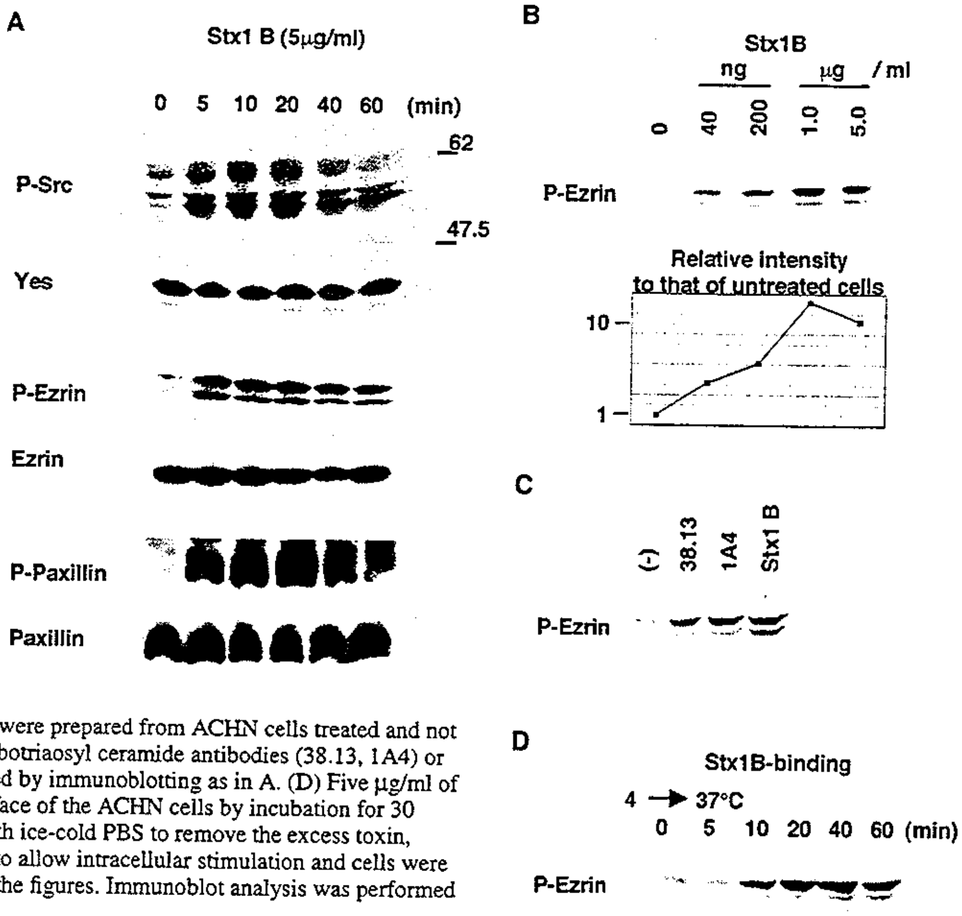

Fig. 8. Transient phosphorylation of ezrin in ACHN cells after treatment with the Stx1-B subunit. (A) Total cell extracts were prepared from ACHN cells treated with or without 5 μg/ml of Stx1-B subunit for the indicated periods. After separation on 10% SDS-PAGE gel, the proteins were transferred to a nitrocellulose membrane and immunoblotted using the indicated antibodies. (B) Total cell extracts were prepared from ACHN cells treated with or without different amounts of Stx1-B subunit for 10 minutes and immunoblot analysis was performed using anti-phospho-specific ezrin antibody (P-Ezrin) as in A. Intensity of the phospho-ezrin signals obtained from each sample was quantitated by densitometry and the relative value of each to that of untreated cells (each value/the value of untreated cells) was indicated as a graph (lower panel). (C) Total cell extracts were prepared from ACHN cells treated and not treated with 5 μg/ml each of either anti-globotriaosyl ceramide antibodies (38.13, 1A4) or Stx1-B subunit for 10 minutes and examined by immunoblotting as in A. (D) Five μg/ml of Stx1-B pentamer was bound to the cell surface of the ACHN cells by incubation for 30 minutes at 4°C. After intensive washing with ice-cold PBS to remove the excess toxin, temperature was shifted from 4°C to 37°C to allow intracellular stimulation and cells were incubated for the time periods indicated in the figures. Immunoblot analysis was performed as in A.

Discussion

In this report, we clearly demonstrated that the binding of Stx1-B induces intracellular signals that initiate cytoskeleton remodeling in ACHN renal carcinoma cells, which are related to renal tubular epithelial cells. These signals led to morphological changes and a weakened adhesiveness of the cells. The series of cellular and biological events induced by Stx1-B binding was similar to that which occurs during the course of growth factor-stimulated cell motility (Bretscher, 1989; Leventhal et al., 1997).

Several lines of evidence, including our own, have suggested that Stx directly injures renal tubular epithelial cells. For example, renal tubular epithelial cells express Gb3, which can bind Stx1 and 2 (Boyd and Lingwood, 1989; Kiyokawa et al., 1998; Taguchi et al., 1998; Uchida et al., 1999). In vitro experiments have revealed that Stx1 induces cell death in renal tubular epithelial cells through protein synthesis inhibition and apoptosis (Karpman et al., 1998; Kiyokawa et al., 1998; Taguchi et al., 1998; Williams et al., 1999). Several clinical studies have indicated the involvement of renal tubular damage during the course of HUS (Kaneko et al., 2001; Takeda et al., 1993). The appearance of apoptotic cells in the renal tubules of the kidney in HUS patients, accompanied by STEC infection, further indicates that renal tubular injury does occur in the kidneys of HUS patients (Karpman et al., 1998; Taguchi et al., 1998).

The essential cytotoxicity of Stx is generally thought to arise from the inhibition of protein synthesis by the Stx-A subunit. However, recent studies have shown that the B-subunit also has biological effects on target cells through a mechanism mediated by intracellular signals upon binding to Gb3 (Katagiri et al., 1999; Kiyokawa et al., 2001; Mangeney et al., 1993; Mori et al., 2000; Taga et al., 1997). Although Stx1-B-induced intracellular signals are known to mediate apoptosis in Burkitt's lymphoma cells, their biological effect on other cell species has not been clarified. The data presented in this study extend previous observations and indicate that Stx1-B-induced intracellular signals induce cytoskeleton remodeling, resulting in morphological changes in the target cells. As previously reported, the simultaneous addition of Stx1-B subunits enhances the cytotoxic effect of Stx1 holotoxins on ACHN cells, suggesting a synergism between A-subunit-mediated protein synthesis inhibition and B-subunit-mediated intracellular signals on the cytotoxicity observed in target cells (Katagiri et al., 2001). Although the biological significance of Stx1-B-induced cytoskeletal remodeling in target cells in vivo is not presently known, this process might participate in Stx-induced cell injury, thereby playing a role in the development of complications associated with STEC infection, such as HUS.

Gb3 acts as functional receptor for Stx, but the natural ligand of this lipid and its normal physiological role are unknown. Upon binding with its natural ligand, Gb3 might mediate intracellular signals leading to cytoskeletal remodeling,

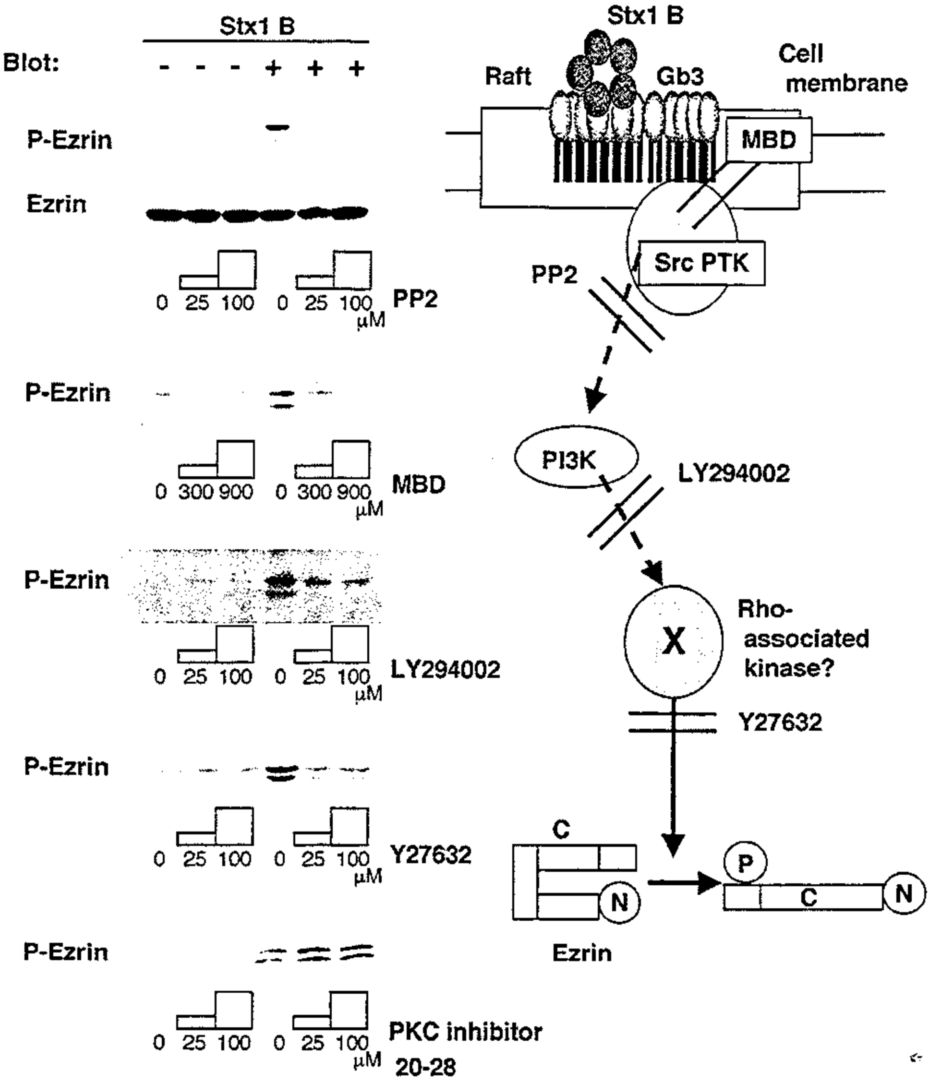

Fig. 9. Effect of inhibitors on the Stx1-B-subunit-mediated phosphorylation of ezrin. ACHN cells were preincubated with the inhibitors shown in the figure for three hours. The concentrations of 300 and 900 μM for MBD and 25 and 100 μM for other inhibitors were used. After treatment with the Stx1-B subunit for 5 minutes, cell extracts were prepared, and immunoblotting for phospho-specific ezrin was performed as described in Fig. 8. In parallel, each sample was examined using an anti-ezrin antibody to confirm that the protein amounts in each lane were comparable (only the result for PP2 is shown in the second panel from the top). In the right panel, the effect of each inhibitor is schematically presented.

participating in the development and organization of kidney tissue. Therefore, our observation might provide an in vitro model for research on lipid-receptor-mediated signaling systems for cytoskeletal remodeling.

Stx1-B binding induces the phosphorylation of ezrin, a linker protein that connects the plasma membrane and the actin cytoskeleton and is involved in cell adhesion and the formation of the free-surface domain of plasma membranes, especially in the ruffling and organization of microvilli (Berryman et al., 1995; Bretscher et al., 1997; Chen et al., 1995; Crepadi et al., 1997; Kondo et al., 1997; Takeuchi et al., 1994; Tsukita and Yonemura, 1999). Stx1-B-induced ezrin phosphorylation was inhibited both by MBD (which disturbs the structure of lipid rafts) and by the Src family PTK inihibitor PP2. Furthermore, we previously reported that Gb3 is mainly located on lipid rafts in the cell membrane, and that Stx1-B binding to Gb3 induces a clustering of the lipid rafts, leading to the activation of Src family PTK (which is anchored to the inner layer of the lipid rafts) possibly by aggregation-mediated kinase auto-phosphorylation (Katagiri et al., 1999; Mori et al., 2000). Thus, our data indicate that the lipid-raft-mediated activation of Src family PTK might play an important role in the phosphorylation of ezrin during the course of Stx-induced cytoskeleton remodeling. In addition to MBD and PP2, we also found that the inhibition of both PI3K and ROCK by their specific inhibitors abolished the Stx1-B-mediated phosphorylation of ezrin, suggesting that these molecules are located downstream from Src family PTK in the signaling cascade and participate in the Stx1-B-mediated phosphorylation of ezrin.

Several molecules have been postulated to be responsible for the phosphorylation of ezrin. For example, the Ras superfamily small G-proteins Rho, Rac and Cdc42 have been shown to be responsible for the formation of focal contact, lamellipodia and filopodia, respectively (Van Aelst and D'Souza-Schorey, 1997; Mackay and Hall, 1998). During these processes, the ERM proteins are thought to be located downstream of the small G-proteins (Bretscher et al., 1997; Matsui et al., 1998; Shaw et al., 1998; Tsukita and Yonemura, 1999). Furthermore, it has been shown that ROCK phosphorylates the C-terminal threonines of ERM proteins, regulating their head-to-tail association in in vitro experiments (Matsui et al., 1998).

We also know that myotonic dystrophy kinase-related Cdc42-binding kinase (MRCK) is a candidate for the kinase that phosphorylates ERM proteins at filopodia (Nakamura et al., 2000). In the case of Merlin, which is closely related to the ERM proteins, p21-activated kinase 2 (PAK2), a downstream effector of Rac and Cdc42, has been postulated as a candidate for the kinase that phosphorylates this protein (Kissil et al., 2002). Consistent with the above observations, we report here that the ROCK inhibitor Y27632 inhibited the Stx1-B-stimulated phosphorylation of ezrin, suggesting that ROCK is at least one of the kinases responsible for ezrin phosphorylation in Stx1-B-induced cytoskeletal remodeling. In addition, Rac and Cdc42 might also be involved in the process, as Stx1-B stimulation induces the extension of lamellipodia- and

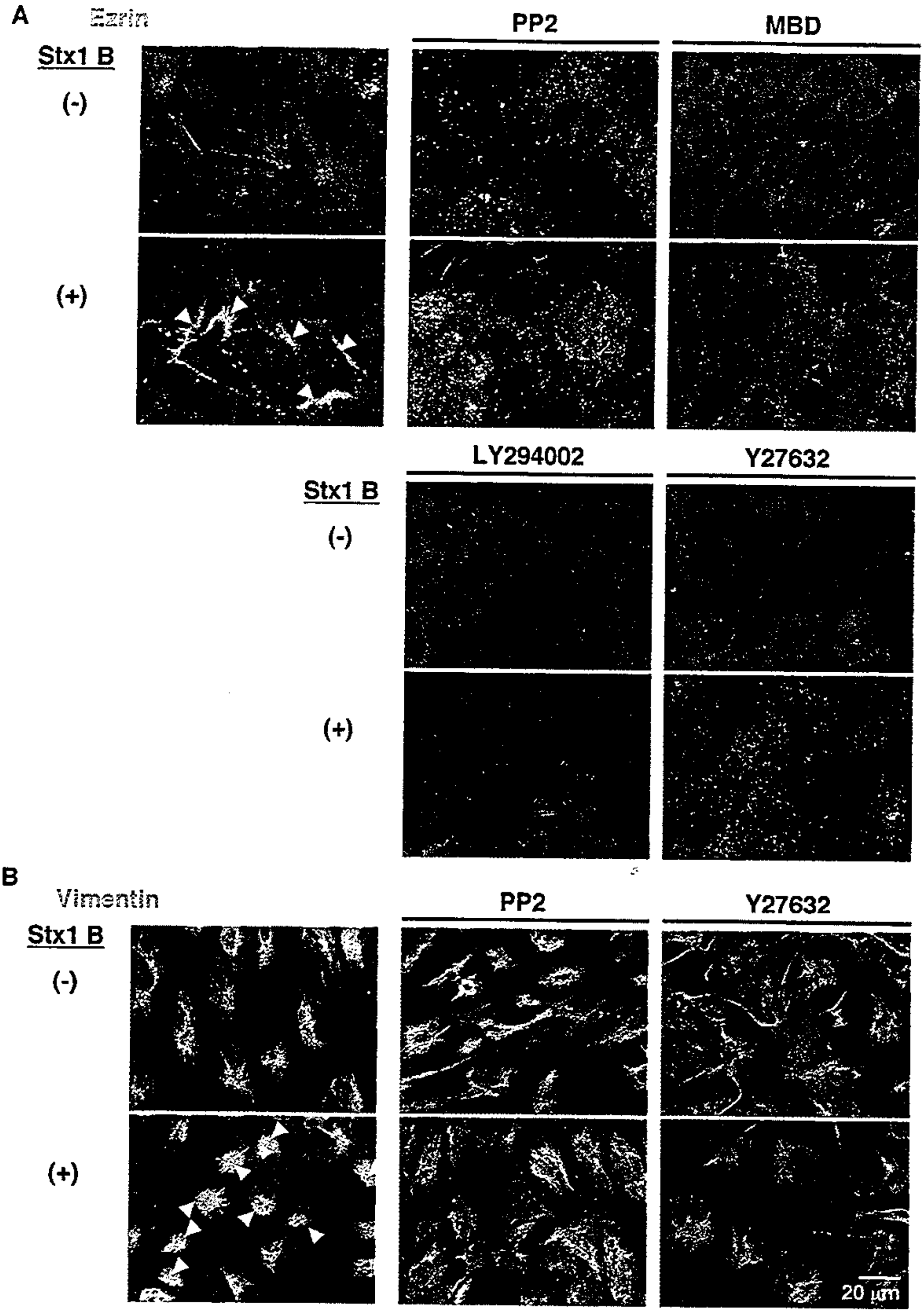

Fig. 10. Effect of inhibitors on the Stx1-B-subunit-mediated clustering of ezrin and vimentin. (A) ACHN cells were preincubated with the inhibitors shown in the figure for three hours. The concentrations of 900 µM for MBD and 100 µM for other inhibitors were used. After treatment with the Stx1-B subunit for 10 minutes, the cells were fixed and stained with anti-ezrin monoclonal antibody (green) followed by counterstaining with DAPI (blue) as in Fig. 2. Results are representative of three independent experiments. The clustering of ezrin was indicated by arrowhead. (B) ACHN cells pre-incubated with inhibitors as in A were treated with the Stx1-B for 30 minutes and stained with anti-vimentin monoclonal antibody (green) as in A.

filopodia-like structures. Further experiments investigating the involvement of small G-proteins and their downstream kinases in the Stx1-B-induced signaling system of cytoskeletal remodeling are now underway.

Conversely, it has been suggested that ezrin was a downstream effector of PKCα during the course of integrin-mediated cell migration (Ng et al., 2001). PKCθ is a major kinase specific for moesin, a family protein of ezrin (Pietromonaco et al., 1998). PKCθ is involved in regulating the localization and association of CD44 and ezrin during cell motility and invasion (Legg et al., 2002; Stapleton et al., 2002). As shown in this study, however, the PKC-inhibitors did not affect the Stx1-B-stimulated phosphorylation of ezrin. Our data might indicate that PKCs are not essential for the Stx1-B-induced phosphorylation of ezrin in our experimental system.

In addition to the phosphorylation of ezrin, we also observed changes in the distributions of several molecules, including FAK, paxillin, vimentin, cytokeratin and tubulins, all of which contribute to the organization of the cytosleleton. The molecular mechanism responsible for the above-described redistribution of cytoskeletal molecules has not yet been clarified. However, as observed in the present study, treatment with the ROCK inhibitor Y27632 abolished the Stx1-B-stimulated relocalization of vimentin, suggesting the involvement of ROCK in the Stx1-B-induced redistribution of vimentin. The ability of ROCK to phosphorylate vimentin in vitro and in vivo (Goto et al., 1998; Kosako et al., 1999) might support this idea.

In conclusion, Stx1-B-induced intracellular signals mediate the remodeling of a variety of cytoskeletal organizing proteins, resulting in changes in cell morphology. Although additional studies are clearly necessary, further investigation of the mechanism of Stx1-B-mediated cytoskeletal remodeling should provide an in vitro model for future research on the pathogenesis of Stx-mediated cell injury as well as the role of lipid raft-mediated cell signaling in cytoskeletal remodeling.

This work was supported in part by Health and Labour Sciences Research Grants from the Ministry of Health, Labour and Welfare of Japan and MEXT. KAKENHI 15019129, JSPS. KAKENHI 15390133 and 15590361. This work was also supported by a grant from the Japan Health Sciences Foundation for Research on Health Sciences Focusing on Drug Innovation. Additional support was provided by a grant from Sankyo Foundation of Life Science. We thank M. Sone and S. Yamauchi for their excellent secretarial works. We thank S. Hakomori and Otsuka Assay Laboratories for gifting anti-Gb3 mAb 1A4.

References

Andreoli, C., Martin, M., le Borgne, R., Reggio, H. and Mangeat, P. (1994). Ezrin has properties to self-associate at the plasma membrane. *J. Cell Sci.* **107**, 2509-2521.

Arpin, M., Algrain, M. and Louvard, D. (1994). Membrane-actin microfilament connections: an increasing diversity of players related to band 4.1. *Curr. Opin. Cell Biol.* **6**, 136-141.

Berryman, M., Gary, R. and Bretscher, A. (1995). Ezrin oligomers are major cytoskeletal components of placental microvilli: a proposal for their involvement in cortical morphogenesis. *J. Cell Biol.* **131**, 1231-1242.

Boyd, B. and Lingwood, C. (1989). Verotoxin receptor glycolipid in human renal tissue. *Nephron* **51**, 207-210.

Bretscher, A. (1989). Rapid phosphorylation and reorganization of ezrin and spectrin accompany morphological changes induced in A-431 cells by epidermal growth factor. *J. Cell Biol.* **108**, 921-930.

Bretscher, A., Gary, R. and Berryman, M. (1995). Soluble ezrin purified from placenta exists as stable monomers and elongated dimers with masked C-terminal ezrin-radixin-moesin association domains. *Biochemistry* **34**, 16830-16837.

Bretscher, A., Reczek, D. and Berryman, M. (1997). Ezrin: a protein requiring conformational activation to link microfilaments to the plasma membrane in the assembly of cell surface structures. *J. Cell Sci.* **110**, 3011-3018.

Burridge, K., Turner, C. E. and Romer, L. H. (1992). Tyrosine phosphorylation of paxillin and pp125FAK accompanies cell adhesion to extracellular matrix: a role in cytoskeletal assembly. *J. Cell Biol.* **119**, 893-903.

Chen, J., Cohn, J. A. and Mandel, L. J. (1995). Dephosphorylation of ezrin as an early event in renal microvillar breakdown and anoxic injury. *Proc. Natl. Acad. Sci. USA* **92**, 7495-7499.

Crepaldi, T., Gautreau, A., Comoglio, P. M., Louvard, D. and Arpin, M. (1997). Ezrin is an effector of hepatocyte growth factor-mediated migration and morphogenesis in epithelial cells. *J. Cell Biol.* **138**, 423-434.

Glogauer, M., Arora, P., Yao, G., Sokholov, I., Ferrier, J. and McCulloch, C. A. (1997). Calcium ions and tyrosine phosphorylation interact coordinately with actin to regulate cytoprotective responses to stretching. *J. Cell Sci.* **110**, 11-21.

Goto, H., Kosako, H., Tanabe, K., Yanagida, M., Sakurai, M., Amano, M., Kaibuchi, K. and Inagaki, M. (1998). Phosphorylation of vimentin by Rho-associated kinase at a unique amino-terminal site that is specifically phosphorylated during cytokinesis. *J. Biol. Chem.* **273**, 11728-11736.

Heacock, C. S. and Bamburg, J. R. (1983). The quantification of G- and F-actin in cultured cells. *Anal. Biochem.* **135**, 22-36.

Heiska, L., Alfthan, K., Gronholm, M., Vilja, P., Vaheri, A. and Carpen, O. (1998). Association of ezrin with intercellular adhesion molecule-1 and -2 (ICAM-1 and ICAM-2). Regulation by phosphatidylinositol 4, 5-bisphosphate. *J. Biol. Chem.* **273**, 21893-21900.

Hirao, M., Sato, N., Kondo, T., Yonemura, S., Monden, M., Sasaki, T., Takai, Y., Tsukita, S. and Tsukita, S. (1996). Regulation mechanism of ERM (ezrin/radixin/moesin) protein/plasma membrane association: possible involvement of phosphatidylinositol turnover and Rho-dependent signaling pathway. *J. Cell Biol.* **135**, 37-51.

Kaneko, K., Kiyokawa, N., Ohtomo, Y., Nagaoka, R., Yamashiro, Y., Taguchi, T., Mori, T., Fujimoto, J. and Takeda, T. (2001). Apoptosis of renal tubular cells in Shiga-toxin-mediated hemolytic uremic syndrome. *Nephron* **87**, 182-185.

Kaplan, B. S., Cleary, T. G. and Obrig, T. G. (1990). Recent advances in understanding the pathogenesis of the hemolytic uremic syndromes. *Pediatr. Nephrol.* **4**, 276-283.

Karpman, D., Hakansson, A., Perez, M. T., Isaksson, C., Carlemalm, E., Caprioli, A. and Svanborg, C. (1998). Apoptosis of renal cortical cells in the hemolytic-uremic syndrome: in vivo and in vitro studies. *Infect. Immun.* **66**, 636-644.

Katagiri, U. Y., Mori, T., Nakajima, H., Katagiri, C., Taguchi, T., Takeda, T., Kiyokawa, N. and Fujimoto, J. (1999). Activation of Src family kinase Yes induced by Shiga toxin binding to globotriaosyl ceramide (Gb3/CD77) in low density, detergent-insoluble microdomains. *J. Biol. Chem.* **274**, 35278-35282.

Katagiri, U. Y., Kiyokawa, N. and Fujimoto, J. (2001). The effect of Shiga toxin binding to globotriaosylceramide in rafts of human kidney cells and Burkitt's lymphomaa cells. *Trends. Glycosci. Glycotech.* **13**, 281-290.

Kissil, J. L., Johnson, K. C., Eckman, M. S. and Jacks, T. (2002). Merlin phosphorylation by p21-activated kinase 2 and effects of phosphorylation on merlin localization. *J. Biol. Chem.* **277**, 10394-10399.

Kiyokawa, N., Taguchi, T., Mori, T., Uchida, H., Sato, N., Takeda, T. and Fujimoto, J. (1998). Induction of apoptosis in normal human renal tubular epithelial cells by *Escherichia coli* Shiga toxins 1 and 2. *J. Infect. Dis.* **178**, 178-184.

Kiyokawa, N., Mori, T., Taguchi, T., Saito, M., Mimori, K., Suzuki, T., Sekino, T., Sato, N., Nakajima, H., Katagiri, Y. U. et al. (2001). Activation of the caspase cascade during Stx1-induced apoptosis in Burkitt's lymphoma cells. *J. Cell. Biochem.* **81**, 128-142.

Knowles, G. C. and McCulloch, C. A. (1992). Simultaneous localization and quantification of relative G and F actin content: optimization of fluorescence labeling methods. *J. Histochem. Cytochem.* **40**, 1605-1612.

Kojio, S., Zhang, H., Ohmura, M., Gondaira, F., Kobayashi, N. and Yamamoto, T. (2000). Caspase-3 activation and apoptosis induction coupled with the retrograde transport of shiga toxin: inhibition by brefeldin A. *FEMS Immunol. Med. Microbiol.* **29**, 275-281.

Kondo, T., Takeuchi, K., Doi, Y., Yonemura, S., Nagata, S. and Tsukita, S. (1997). ERM (ezrin/radixin/moesin)-based molecular mechanism of microvillar breakdown at an early stage of apoptosis. *J. Cell Biol.* **139**, 749-758.

Kosako, H., Goto, H., Yanagida, M., Matsuzawa, K., Fujita, M., Tomono, Y., Okigaki, T., Odai, H., Kaibuchi, K. and Inagaki, M. (1999). Specific accumulation of Rho-associated kinase at the cleavage furrow during cytokinesis: cleavage furrow-specific phosphorylation of intermediate filaments. *Oncogene* **18**, 2783-2788.

Legg, J. W., Lewis, C. A., Parsons, M., Ng, T. and Isacke, C. M. (2002). A novel PKC-regulated mechanism controls CD44 ezrin association and directional cell motility. *Nat. Cell Biol.* **4**, 399-407.

Leventhal, P. S., Shelden, E. A., Kim, B. and Feldman, E. L. (1997). Tyrosine phosphorylation of paxillin and focal adhesion kinase during insulin-like growth factor-I-stimulated lamellipodial advance. *J. Biol. Chem.* **272**, 5214-5218.

Lingwood, C. A. (1996). Role of verotoxin receptors in pathogenesis. *Trends Microbiol.* **4**, 147-153.

Mackay, D. J. and Hall, A. (1998). Rho GTPases. *J. Biol. Chem.* **273**, 20685-20688.

Mangeney, M., Lingwood, C. A., Taga, S., Caillou, B., Tursz, T. and Wiels, J. (1993). Apoptosis induced in Burkitt's lymphoma cells via Gb3/CD77, a glycolipid antigen. *Cancer Res.* **53**, 5314-5319.

Matsui, T., Maeda, M., Doi, Y., Yonemura, S., Amano, M., Kaibuchi, K., Tsukita, S. and Tsukita, S. (1998). Rho-kinase phosphorylates COOH-terminal threonines of ezrin/radixin/moesin (ERM) proteins and regulates their head-to-tail association. *J. Cell Biol.* **140**, 647-657.

McCormack, S. A., Ray, R. M., Blanner, P. M. and Johnson, L. R. (1999). Polyamine depletion alters the relationship of F-actin, G-actin, and thymosin beta4 in migrating IEC-6 cells. *Am. J. Physiol.* **276**, C459-C468.

Minotti, A. M., Barlow, S. B. and Cabral, F. (1991). Resistance to antimitotic drugs in Chinese hamster ovary cells correlates with changes in the level of polymerized tubulin. *J. Biol. Chem.* **266**, 3987-3994.

Montgomery, R. B., Guzman, J., O'Rourke, D. M. and Stahl, W. L. (2000). Expression of oncogenic epidermal growth factor receptor family kinases induces paclitaxel resistance and alters beta-tubulin isotype expression. *J. Biol. Chem.* **275**, 17358-17363.

Mori, T., Kiyokawa, N., Katagiri, Y. U., Taguchi, T., Suzuki, T., Sekino, T., Sato, N., Ohmi, K., Nakajima, H., Takeda, T. et al. (2000). Globotriaosyl ceramide (CD77/Gb3) in the glycolipid-enriched membrane domain participates in B-cell receptor-mediated apoptosis by regulating lyn kinase activity in human B cells. *Exp. Hematol.* **28**, 1260-1268.

Moritz, M. and Agard, D. A. (2001). γ-tubulin complexes and microtubule nucleation. *Curr. Opin. Struct. Biol.* **11**, 174-181.

Nakajima, H., Katagiri, Y. U., Kiyokawa, N., Taguchi, T., Suzuki, T., Sekino, T., Mimori, K., Saito, M., Nakao, H., Takeda, T. et al. (2001). Single-step method for purification of Shiga toxin-1 B subunit using receptor-mediated affinity chromatography by globotriaosylceramide-conjugated octyl sepharose CL-4B. *Protein Expr. Purif.* **22**, 267-275.

Nakamura, N., Oshiro, N., Fukata, Y., Amano, M., Fukata, M., Kuroda, S., Matsuura, Y., Leung, T., Lim, L. and Kaibuchi, K. (2000). Phosphorylation of ERM proteins at filopodia induced by Cdc42. *Gene. Cell.* **5**, 571-581.

Ng, T., Parsons, M., Hughes, W. E., Monypenny, J., Zicha, D., Gautreau, A., Arpin, M., Gschmeissner, S., Verveer, P. J., Bastiaens, P. I. et al. (2001). Ezrin is a downstream effector of trafficking PKC-integrin complexes involved in the control of cell motility. *EMBO J.* **20**, 2723-2741.

Pietromonaco, S. F., Simons, P. C., Altman, A. and Elias, L. (1998). Protein kinase C-theta phosphorylation of moesin in the actin-binding sequence. *J. Biol. Chem.* **273**, 7594-7603.

Richardson, S. E., Karmali, M. A., Becker, L. E. and Smith, C. R. (1988). The histopathology of the hemolytic uremic syndrome associated with verocytotoxin-producing *Escherichia coli* infections. *Hum. Pathol.* **19**, 1102-1108.

Rodgers, W. and Rose, J. K. (1996). Exclusion of CD45 inhibits activity of p56lck associated with glycolipid-enriched membrane domains. *J. Cell Biol.* **135**, 1515-1523.

Serrador, J. M., Alonso-Lebrero, J. L., del Pozo, M. A., Furthmayr, H., Schwartz-Albiez, R., Calvo, J., Lozano, F. and Sanchez-Madrid, F. (1997). Moesin interacts with the cytoplasmic region of intercellular adhesion molecule-3 and is redistributed to the uropod of T lymphocytes during cell polarization. *J. Cell Biol.* **138**, 1409-1423.

Shaw, R. J., Henry, M., Solomon, F. and Jacks, T. (1998). RhoA-dependent phosphorylation and relocalization of ERM proteins into apical membrane/actin protrusions in fibroblasts. *Mol. Biol. Cell* **9**, 403-419.

Simons, K. and Ikonen, E. (1997). Functional rafts in cell membranes. *Nature* **387**, 569-572.

Stapleton, G., Malliri, A. and Ozanne, B. W. (2002). Downregulated AP-1 activity is associated with inhibition of protein-kinase-C-dependent CD44 and ezrin localisation and upregulation of PKC theta in A431 cells. *J. Cell Sci.* **115**, 2713-2724.

Taga, S., Carlier, K., Mishal, Z., Capoulade, C., Mangeney, M., Lecluse, Y., Coulaud, D., Tetaud, C., Pritchard, L. L., Tursz, T. et al. (1997). Intracellular signaling events in CD77-mediated apoptosis of Burkitt's lymphoma cells. *Blood* **90**, 2757-2767.

Taguchi, T., Uchida, H., Kiyokawa, N., Mori, T., Sato, N., Horie, H., Takeda, T. and Fujimoto, J. (1998). Verotoxins induce apoptosis in human renal tubular epithelium derived cells. *Kidney Int.* **53**, 1681-1688.

Takeda, T., Dohi, S., Igarashi, T., Yamanaka, T., Yoshiya, K. and Kobayashi, N. (1993). Impairment by verotoxin of tubular function contributes to the renal damage seen in haemolytic uraemic syndrome. *J. Infect.* **27**, 339-341.

Takeuchi, K., Sato, N., Kasahara, H., Funayama, N., Nagafuchi, A., Yonemura, S., Tsukita, S. and Tsukita, S. (1994). Perturbation of cell adhesion and microvilli formation by antisense oligonucleotides to ERM family members. *J. Cell Biol.* **125**, 1371-1384.

Tsukita, S. and Yonemura, S. (1997). ERM (ezrin/radixin/moesin) family: from cytoskeleton to signal transduction. *Curr. Opin. Cell Biol.* **9**, 70-75.

Tsukita, S. and Yonemura, S. (1999). Cortical actin organization: lessons from ERM (ezrin/radixin/moesin) proteins. *J. Biol. Chem.* **274**, 34507-34510.

Tsukita, S., Oishi, K., Sato, N., Sagara, J., Kawai, A. and Tsukita, S. (1994). ERM family members as molecular linkers between the cell surface glycoprotein CD44 and actin-based cytoskeletons. *J. Cell Biol.* **126**, 391-401.

Tsukita, S., Yonemura, S. and Tsukita, S. (1997). ERM proteins: head-to-tail regulation of actin-plasma membrane interaction. *Trends. Biochem. Sci.* **22**, 53-58.

Turunen, O., Wahlstrom, T. and Vaheri, A. (1994). Ezrin has a COOH-terminal actin-binding site that is conserved in the ezrin protein family. *J. Cell Biol.* **126**, 1445-1453.

Uchida, H., Kiyokawa, N., Horie, H., Fujimoto, J. and Takeda, T. (1999). The detection of Shiga toxins in the kidney of a patient with hemolytic uremic syndrome. *Pediatr. Res.* **45**, 133-137.

Van Aelst, L. and D'Souza-Schorey, C. (1997). Rho GTPases and signaling networks. *Genes. Dev.* **11**, 2295-2322.

Williams, J. M., Lea, N., Lord, J. M., Roberts, L. M., Milford, D. V. and Taylor, C. M. (1997). Comparison of ribosome-inactivating proteins in the induction of apoptosis. *Toxicol. Lett.* **91**, 121-127.

Williams, J. M., Boyd, B., Nutikka, A., Lingwood, C. A., Barnett-Foster, D. E., Milford, D. V. and Taylor, C. M. (1999). A comparison of the effects of verocytotoxin-1 on primary human renal cell cultures. *Toxicol. Lett.* **105**, 47-57.

Yonemura, S., Nagafuchi, A., Sato, N. and Tsukita, S. (1993). Concentration of an integral membrane protein, CD43 (leukosialin, sialophorin), in the cleavage furrow through the interaction of its cytoplasmic domain with actin-based cytoskeletons. *J. Cell Biol.* **120**, 437-449.